

Effects of Strontium on the Physicochemical Characteristics of Hydroxyapatite

S. C. Verberckmoes,¹ G. J. Behets,¹ L. Oste,¹ A. R. Bervoets,¹ L. V. Lamberts,¹ M. Drakopoulos,² A. Somogyi,² P. Cool,³ W. Dorriné,³ M. E. De Broe,¹ P. C. D'Haese¹

¹Department of Nephrology-Hypertension, University of Antwerp, Antwerp, Belgium

²European Synchrotron Radiation Facility, Grenoble, France

³Department of Chemistry, University of Antwerp, Antwerp, Belgium

Received: 15 October 2003 / Accepted: 30 March 2004 / Online publication: 30 July 2004

Abstract. In a previous experimental study using a chronic renal failure rat model, a dose-related multiphasic effect of strontium (Sr) on bone formation was found that could be reproduced in an *in vitro* set-up using primary rat osteoblasts. The results from the latter study allowed us to distinguish between a reduced nodule formation in the presence of an intact mineralization at low Sr-doses (1 µg/ml) and an interference of the element with the hydroxyapatite (HA) formation at high doses (20–100 µg/ml). To further investigate the latter effect of Sr on physicochemical bone mineral properties, an *in vitro* study was set up in which the UMR-106 rat osteosarcoma cell line was exposed to Sr, added to the cell culture medium in a concentration range varying between 0–100 µg/ml. Temporal growth and functionality of the culture was investigated by measurement of the alkaline phosphatase activity and calcium (Ca) concentration in the culture medium (used as an index of Ca-incorporation, i.e., HA formation) at various time points. At the end of the culture period (14 days post-confluence), samples of the mineralized cultures were taken for further analysis using X-ray diffraction (XRD) and Fourier Transform Infra-Red Spectroscopy (FTIR). Synthetic HA doped with various Sr concentrations (based on the cell culture and previous experimental studies and yielding Sr/(Sr+Ca) ratios ranging from 0–60%), was prepared and examined for crystal growth and solubility. Crystal size was assessed using scanning electron microscopy (SEM). Ca incorporation indicated a reduced mineralization in the 20 and 100 µg/ml Sr groups vs. controls. Sr-doped synthetic HA showed a significant dose-dependent reduction in crystal growth, as assessed by SEM, and an increase in solubility, apparent from 12.7% Sr/(Sr+Ca) on. Moreover, in both mineralized cultures and synthetic HA, XRD and FTIR analysis showed a reduced crystallinity and altered crystal lattice at similar concentrations. These new data support our previous *in vivo* and *in vitro* findings and point to a potential physicochemical interference of Sr with HA formation and crystal properties *in vivo*.

Key words: Strontium — Hydroxyapatite — X-ray diffraction — Mineralization — Cell culture

Strontium (Sr) is a trace element that is found in calcareous rocks and ocean water [1, 2]. Moreover, it is a natural component of food and beverages [3]. In line with its chemical analogy to calcium (Ca), Sr is a bone-seeking element and 98% of the total body Sr content can be found in the skeleton [4]. Over the years a substantial amount of research has been performed on the effects of Sr on bone and both beneficial [5–8] and deleterious [9–13] effects have been reported depending on the Sr dose administered and the presence or absence of renal failure. Indeed, in rats with normal renal function, daily Sr administration via the drinking water (as the chloride compound) at doses varying between 0.19–0.34% during 9 weeks resulted in an increased bone volume [5–7, 14] whereas higher Sr doses (≥0.40%) induced a mineralization defect [6, 14]. Several decades ago evidence for a rachitogenic potential of dietary Sr was presented in chickens with normal renal function by demonstrating an interference of the element with the calcium absorption and renal vitamin D synthesis [9, 10]. Based on the element's ability to enhance bone volume, the possible use of Sr, as the ranelate compound, in the treatment of osteoporosis is currently evaluated in various experimental studies and clinical trials [15–18]. Previous data from our group indicated that Sr, administered via the drinking water (0.34% as the Sr-chloride compound) to chronic renal failure rats during 12 weeks, induces a bone lesion histologically characterized as osteomalacia [13]. Moreover, further experiments in this rat model revealed the effect of Sr on bone to be complex and dose-dependent. Here it was shown that a low Sr dose (0.03% in the drinking water) led to the development of a bone disease with the histologic characteristics of an adynamic bone disease, while at the intermediate dose (0.075%) no difference

with vehicle-treated rats was seen. At the highest Sr dose (0.15%) the development of severe osteomalacic lesions was confirmed [12]. Furthermore, in a recent *in vitro* experiment using primary osteoblasts isolated from fetal rat calvaria, we also observed a complex multiphasic effect of the element. Indeed, at low doses (1.0 $\mu\text{g/ml}$ Sr in the culture medium) a reduced nodule formation was noticed in the presence of an intact mineralization; at intermediate concentrations (5 $\mu\text{g/ml}$) no effect was seen; at high concentrations (20–100 $\mu\text{g/ml}$) an intact nodule formation was accompanied by a reduced mineralization [19]. These results suggest an effect of the element at the level of cell function/differentiation at low doses and a physicochemical interference with the hydroxyapatite formation at high doses. To further investigate this latter effect, the present *in vitro* study, using both the mineralizing UMR-106 osteosarcoma cell line and synthetically prepared hydroxyapatite, was set up. The influence of different Sr doses (1–100 $\mu\text{g/ml}$) on the physicochemical characteristics of the deposited mineral was investigated *in vitro* under well-controlled conditions using established techniques such as Fourier Transform Infra Red spectroscopy (FTIR) and micro-X-ray diffraction (XRD) analysis. In this study we were able to show the existence of a physicochemical interference of high Sr concentrations with the bone mineral formation at both the level of mineralizing osteoblast cell cultures and synthetic hydroxyapatite.

Materials and Methods

Cell Culture

UMR-106 cells were seeded at 10^4 cells/cm² in 175 cm² culture flasks (Sarstedt, Essen, Belgium) and incubated in α -MEM (Invitrogen; Merelbeke; Belgium) medium supplemented with 50 $\mu\text{g/ml}$ ascorbic acid (Sigma, Bornem, Belgium). At confluence the cultures were divided in 5 different groups (6 independent cultures/group) and exposed to various Sr concentrations (SrCl₂·6H₂O; Merck; Leuven; Belgium) i.e. 0, 1, 5, 20 and 100 $\mu\text{g/ml}$ Sr²⁺ during 2 weeks. The choice of the concentrations correspond to these used in previous cell culture and experimental studies and cover serum concentrations found in osteoporotic patients treated with 1–2 g Sr-ranelate/day [17]. During the culture period the medium was enriched with 2 mM β -glycerolphosphate (Sigma, Bornem, Belgium) to induce mineralization. Cultures were refreshed 3 times per week. During each refreshment, samples of the cell culture medium were collected and stored at -80°C for the measurement of alkaline phosphatase and Ca-incorporation [19]. At the end of the culture period (2 weeks post-confluence) 3 out of the 6 mineralized cultures per group were washed three times with demineralized water, scraped off, pooled and centrifuged to obtain a dense pellet which was subsequently dried overnight at 105°C . These samples were then stored at room temperature until XRD analysis. The remaining 3 cultures were washed with PBS and decalcified in 0.6 N HCl during 24 h to assess the Ca-deposition.

Alkaline Phosphatase Activity

Alkaline phosphatase activity in the conditioned culture medium was determined spectrophotometrically by measure-

ment of the release of *p*-nitro phenol from *p*-nitro phenol-phosphate. The enzyme activity was determined as the change in absorbance at 405 nm over a 10-minutes period. This procedure is based on the kinetic method for measuring total alkaline phosphatase acknowledged by the International Federation of Clinical Chemistry (IFCC) [20].

Ca Incorporation/Deposition

Samples of the culture medium were taken before and after each incubation period to measure the Ca concentration. The decrease in the Ca concentration in the culture medium after incubation was used as a measure of Ca incorporation into the mineralized nodules, i.e., hydroxyapatite formation [19]. This method allows a follow-up of mineralization in function of time in one and the same cell culture without the need to sacrifice it. After integration over the different time points, the Ca incorporation was expressed as the absolute amount Ca incorporated during the incubation period [area under the time-concentration curve (AUC) of 6 time points; 2 weeks]. The AUC of the Ca incorporation was correlated with the Ca-deposition, measured as the amount of Ca released from the cell culture after a 24-h treatment with 0.6 M HCl at the end of the culture period. Ca was determined by means of flame atomic absorption spectrometry using a Perkin Elmer Mod. 372 instrument (Perkin Elmer Corporation; Ueberlingen; Germany) by a modification of the technique of Hansen [21]. To overcome the problem of chemical interference due to the presence of phosphate and high salt content of the samples, 1/50 dilutions of the samples were made in 0.1% La(NO₃)₃.

Sr Determination

Measurement of Sr in the different samples was done using a Zeeman 3030 atomic absorption spectrometer equipped with an HGA-600 graphite furnace (Perkin Elmer Corporation; Ueberlingen; Germany) as previously described in detail [22]. With this method, atomization was performed from the wall of pyrolytically coated graphite tubes. Calibration was performed against matrix-matched calibration curves. The samples were diluted in a 0.5 ml/l TritonX-100-1 ml/l HNO₃ solution.

Hydroxyapatite Synthesis

Hydroxyapatite was synthesized at room temperature by means of a modified wet method previously reported by Sun et al. [23]. Two hundred ml of a 0.5 M CaCl₂ solution was mixed with 75 ml 0.8 M NaH₂PO₄ after which 5 ml of a 12 M NaOH solution was added to precipitate the hydroxyapatite. After curing during 1 week the precipitate was washed 3 times with demineralized water and dried at 105°C overnight. Using this procedure, hydroxyapatite containing various amounts of Sr, replacing Ca on a molar base, was obtained that theoretically resulted in apatitic mineral containing 0, 0.6, 3.2, 12.7, 60 and 100% Sr/(Sr + Ca), respectively. The actual Sr content of the synthetic hydroxyapatite was determined using the above-mentioned methodology. Here, the Sr concentrations applied with the exception of 100% Sr/(Sr + Ca) were based on the medium concentrations used in the *in vitro* osteoblast cell culture experiment, where 0, 0.6, 3.2, 12.7 and 60% Sr/(Sr + Ca) correspond with 0, 1, 5, 20 and 100 $\mu\text{g/ml}$ Sr in the culture medium, respectively.

Solubility/Crystal-Growth Experiments

The solubility in different solutions of the synthetic apatites was studied by exposing 100 mg of apatite to 20 ml bicarbonate solution (0.02 M HCO₃⁻, pH 7.4) during 24 h at 37°C . Using a validated method, inorganic phosphate release from the mineral was used as a measure of crystal solubility [24].

Similarly, crystal growth was studied under physiological conditions by exposing 100 mg apatite to 20 ml α -MEM medium, supplemented with 2 mM β -glycerolphosphate at 37°C during 24 h. Here, phosphate consumption was used as a measure of crystal growth [24].

To quantify the solubility and crystal growth after the incubation period, the samples were centrifuged at 3000 rpm for 15 minutes after which the inorganic phosphorus concentration was measured. Free phosphorus was assessed using the "Inorganic Phosphorus Kit" (Sigma, Bornem, Belgium) based on the method of Fiske and Subbarow [25].

Micro-X-Ray Diffraction (XRD)

X-ray diffraction was carried out at the European Synchrotron Radiation Facility (ESRF) in Grenoble (France) at beam line ID18F dedicated to micro-fluorescence and micro-diffraction [26, 27]. An unfocused, monochromatic beam of 1 mm² cross-section was used to illuminate the sample, mounted on a translation stage for positioning. A high-resolution camera placed at a short distance (a few cm) behind the sample was used to take a radiograph thus facilitating the *in situ* morphological identification.

A 2 mm vertical by 7 mm horizontal micro-beam with a flux of $5 \cdot 10^9$ photons/sec. and a 0.729 Å wavelength was generated using a compound refractive lens. The micro-diffraction patterns were observed with a Fuji Photonics low temp CCD detector with a recording q range of 0.016–4.0 nm⁻¹. Here q is the scattering vector ($q = 2\pi\sin\theta/\lambda$) wherein θ is the scattering angle and λ is the wavelength of incident radiation ($\lambda = 0.729$ Å).

Integration of the obtained XRD patterns to d-spacing format ($d = \text{interplanar distance}$) was done using the X-ray diffraction software package FIT2D developed by Hammersley et al. [28]. Comparison with the reference spectra from the powder diffraction database PDF-2 (International Centre of Diffraction Data, ICDD, USA) was performed after background correction of the integrated XRD-spectra in order to eliminate interference of amorphous phases present in the sample.

Fourier Transform Infra Red Spectroscopy (FTIR)

To identify and characterize the various samples of mineralized cell cultures and synthetic hydroxyapatites, FTIR analysis of the ν_3 and ν_4 vibrations of the apatitic phosphate domain was performed. After mixing the air-dried samples with potassium bromide and pelleting, FTIR spectra were recorded on a Nicolet 20 DXB FTIR-spectrometer (Nicolet Instrument Corporation, Madison WI, USA). 1000 scans were taken in the mid-IR-range (400–4000 cm⁻¹). Deconvolution of the recorded ν_3 and ν_4 vibrations of the phosphate domain of the FTIR-spectra was performed using the software package PeakFit (PeakFit v4, Systat Software UK Limited, London, UK) to increase the resolution and to evaluate overlapping bands. Second derivative peak positions were used as input of the peak position into the deconvolution software. As a deconvolution parameter, a band width of 10 cm⁻¹ and 8 cm⁻¹ was used for the synthetic hydroxyapatite and cell culture samples, respectively.

Scanning Electron Microscopy

To investigate the effect of Ca substitution by Sr on the hydroxyapatite crystal size, the various Sr-doped synthetic hydroxyapatite samples were analyzed on a JEOL JSM 6300 scanning electron microscope. Hereto, mineral samples were positioned onto double sided conducting graphite adhesive tape (SPI supplies division of Structure Probe Inc., West Chester, PA, USA) mounted on a polycarbonate support and inserted into the electron microscope. Due to the small sample

size (few microns) and the use of the conducting double-sided adhesive tape there was no need to coat the samples with a conducting graphite layer. Using the same apparatus the elemental composition of the deposited mineral of air dried cell cultures was determined by means of the Electron Probe X-ray Micro Analysis (EPXMA).

Quantification of the crystal sizes was performed using digital image analysis software (KS-400, Kontron Embedded Computer AG, Munchen, Germany) based on the images obtained by electron microscopy.

Statistics

Data are expressed as mean \pm SD unless otherwise stated. For each of the various study parameters, the various study groups (i.e., different Sr concentrations) vs. the control group (0 $\mu\text{g/mL}$ Sr) were compared by ANOVA. If more than two groups were compared, a post-hoc Bonferroni-test was applied to correct for the number of comparisons. Statistical significance was obtained when $P < 0.05$ at a two-tailed level.

Results

Validation of Mineralizing Osteoblast Cell Culture and Synthetic Hydroxyapatite

Cells seeded at 5000 cells/cm² in 6-well culture plates reached confluence within 5 days. After addition of 2 mM of β -glycerolphosphate to the culture medium, alkaline phosphatase activity increased and mineralization was observed from day 3 post-confluence on. XRD-spectra of the deposited mineral revealed a pattern, typical for hydroxyapatite [$\text{Ca}_{10}(\text{PO}_4)_6(\text{OH})_2$] (Fig. 1), corresponding with the mineral phase found in bone. Moreover, comparison of the FTIR spectra of the *in vitro* deposited mineral with those of synthetic Ca hydroxyapatite and pulverized animal bone revealed the typical absorbance peaks of hydroxyapatite at 1030, 600 and 560 cm⁻¹ (data not shown), confirming the XRD-data. These results present evidence that the *in vitro* formed mineral is hydroxyapatite, the main mineral compound of bone.

Mineral produced by the wet method described above [23] in which theoretically 0, 0.6, 3.2, 12.7, 60% and 100% of the Ca is replaced by Sr, was identified to be hydroxyapatite by both XRD (Fig. 1) and FTIR (Fig. 2). The actual Ca and Sr content was also measured in the hydroxyapatite samples after destruction with concentrated HNO₃ yielding molar Sr/(Sr+Ca) ratios of 0, 1.4, 8.4, 16.6, 65% and 100%, respectively, approaching the theoretical values.

Effect of Sr on the In Vitro Mineralization

Data on the Ca incorporation clearly show a significantly reduced mineralization in the groups treated with the 20 and 100 $\mu\text{g/ml}$ Sr for all investigated time points vs. the control group ($P < 0.05$; Fig. 3A). This is reflected by the AUC (271.4 ± 3.1 and 90.0 ± 5.3 vs. 347.3 ± 6.2 μg incorporated Ca per well; $P < 0.05$;

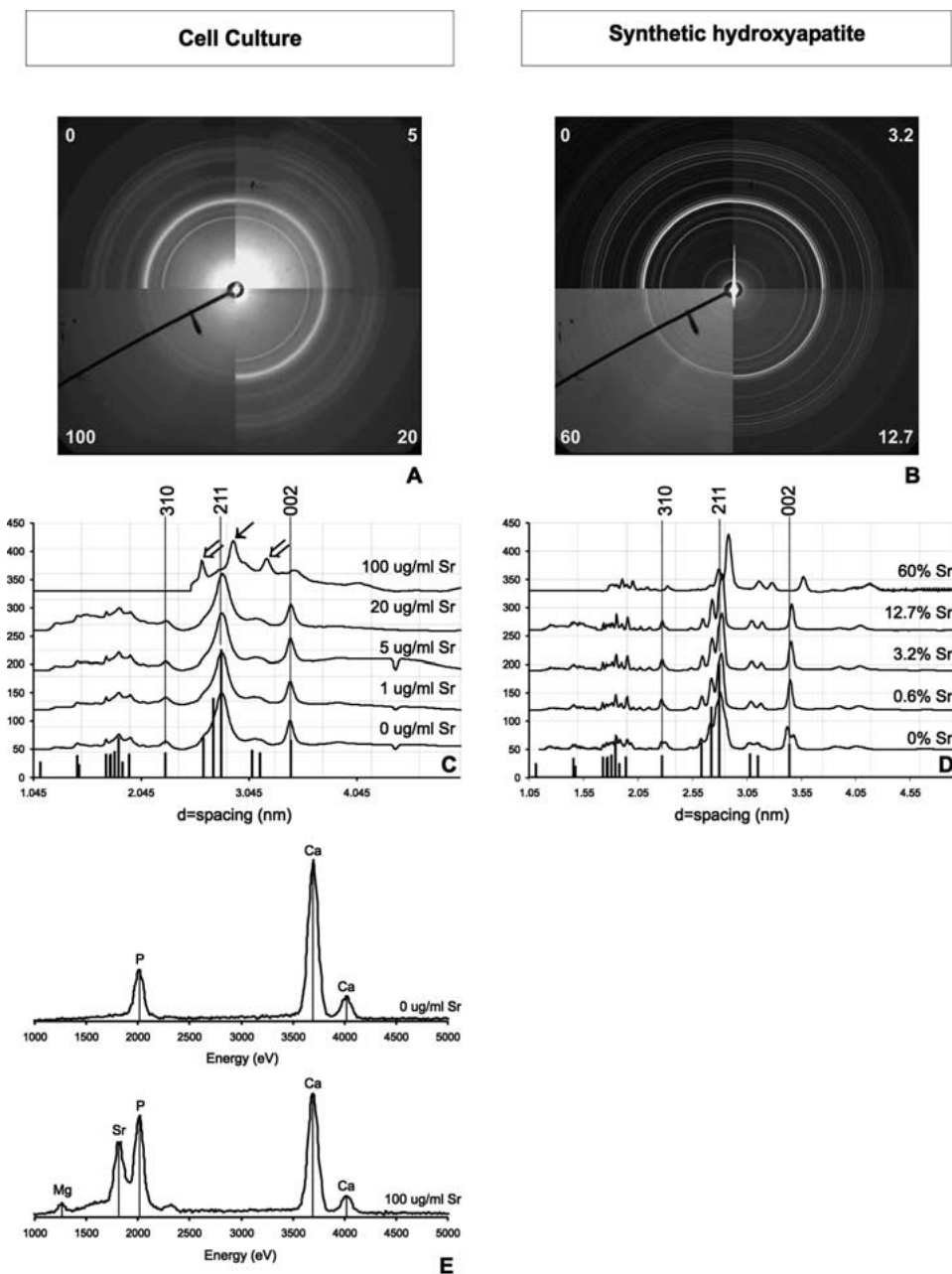


Fig. 1. X-ray diffractograms of (A) mineralized cell cultures (treated with 0, 5, 20 and 100 $\mu\text{g/ml}$ Sr) and (B) synthetic hydroxyapatite (doped with 0, 3.2, 12.7 and 60 mol% Sr) indicate a reduced crystallinity of the mineral phase in the samples with the highest Sr-concentration. Peak positions and heights of the integrated XRD spectra were sent to the ICDD international powder diffraction database to identify the mineral phases present in the samples. The spectra expressed as d-spacing (nm) of mineralized UMR-106 cell cultures and synthetic hydroxyapatite show characteristics of the diffraction pattern of hydroxyapatite $[\text{Ca}_{10}(\text{PO}_4)_6(\text{OH})_2]$ found in the database PDF-2 of the ICDD (represented as line spectra). In cell cultures treated with 100 $\mu\text{g/ml}$ Sr, the mineralization defect gave rise to a very low abundant additional mineral phase composed of whitlockite $[(\text{Ca},\text{Mg})_3(\text{PO}_4)_2]$ (double arrows) and Ca-Sr-hydroxyapatite $[\text{Ca}_2\text{Sr}_8(\text{PO}_4)(\text{OH})_2]$ (single arrow). EPXMA of this latter group revealed the presence of magnesium, hereby confirming the presence of whitlockite in these samples (E).

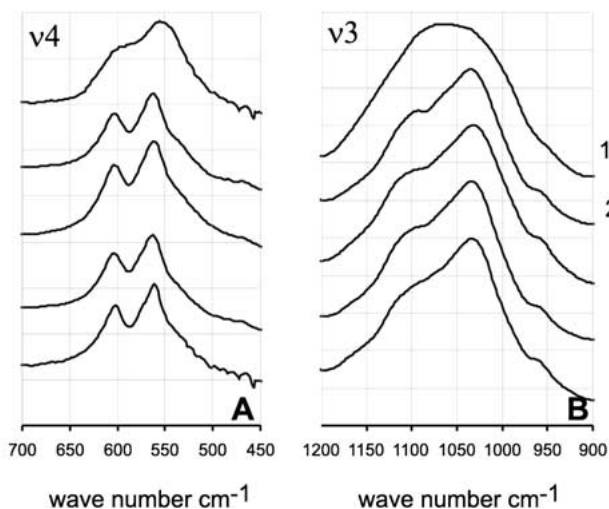
Fig. 4A) as well as by the cellular Ca deposition measured as the amount of Ca that is released after HCl treatment of the mineralized cultures (200.6 ± 21.6 , 8.0 ± 3.2 vs. 293.4 ± 25.6 μg Ca per well; $P < 0.05$; Fig. 4B). No differences in alkaline phosphatase activity among the different treatment groups could be observed during the whole study period (Fig. 3B).

Effect of Sr on the Crystal Growth and Solubility

Phosphorus consumption from the medium was used as a measure of crystal growth [24]. At low Sr concentrations in the synthetic hydroxyapatite (0.6, 3.2 and 12.7%) no statistical significant differences in crystal

growth versus the control group were observed. A significantly reduced phosphorus consumption was only seen for the groups in which 60% of the Ca content was replaced by Sr (115.4 ± 19.7 vs. 188.9 ± 19.2 μg P; $P < 0.05$; Fig. 4C). Complementary results were obtained when the solubility of the crystals was investigated. Similar to the crystal growth experiments, a known amount of hydroxyapatite was incubated overnight in a HCO_3^- buffer at pH 7.4 where after phosphorus release from these crystals was used as a measure of mineral solubility. At low Sr concentrations no effect on crystal solubility could be observed. At high concentrations (12.7–60% Sr), however, a significant increase in phosphorus release versus the control group was noted

Cell Culture



Synthetic hydroxyapatite

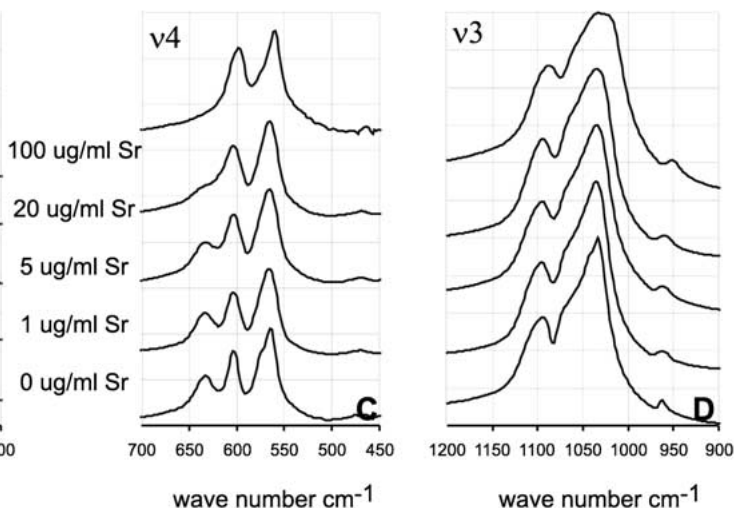


Fig. 2. FTIR spectra of the ν_4 (500–650 cm^{-1}) and ν_3 (950–1150 cm^{-1}) vibrations of the apatitic PO_4 -domain of the mineralized cell cultures (A, B) and synthetic hydroxyapatite (C, D), respectively. All spectra show the main peaks, characteristic of hydroxyapatite with the exception of cultures

treated with 100 $\mu\text{g/ml}$ where a very amorphous mineral phase was found, as indicated by the very unsharp IR-peaks. The peak shift towards smaller wave numbers observed in both cell culture and apatite treated with the highest Sr-concentrations may indicate a disturbed crystal lattice organization.

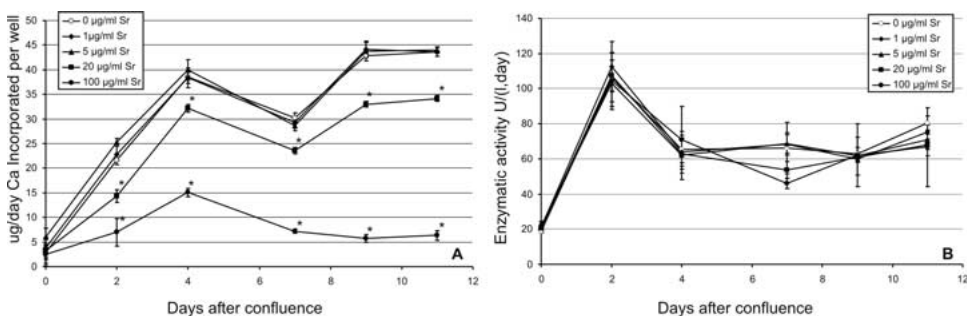


Fig. 3. Time evolution of (A) Ca-incorporation and (B) medium alkaline phosphatase activity for the different groups under study. No difference in alkaline phosphatase activity was found between the various treatment groups while a significantly reduced Ca-incorporation was found for the cultures treated with 20 and 100 $\mu\text{g/ml}$ Sr ($*P < 0.05$ vs. control group).

(89.5 ± 3.4 , 169.7 ± 5.3 vs. 71.3 ± 5.0 $\mu\text{g P}$; $P < 0.05$; Fig. 4D).

XRD Analysis

Comparison of the integrated XRD-spectra of the mineralized cell cultures exposed to 0, 1 and 5 $\mu\text{g/ml}$ Sr with those from the powder diffraction database PDF-2 (International Centre of Diffraction Data, USA) revealed the mineral to be Ca-hydroxyapatite [$\text{Ca}_{10}(\text{PO}_4)_6(\text{OH})_2$] (Fig. 1A and C). Analysis of the cell culture treated with 20 $\mu\text{g/ml}$ Sr, however, indicated the deposited mineral to be $\text{Ca}_9\text{Sr}(\text{PO}_4)_6(\text{OH})_2$ in which 1 Ca-ion out of 10 is substituted by 1 Sr-ion. In the group treated with 100 $\mu\text{g/ml}$ Sr, the deposited mineral revealed a diffuse XRD pat-

tern (Fig. 1A), characteristic for a non-crystalline, amorphous precipitate. Moreover, in the latter XRD-pattern the very faint thin lines pointed to phases other than Ca-hydroxyapatite that could be identified using the powder diffraction database as a mixture of whitlockite [$(\text{Ca},\text{Mg})_3(\text{PO}_4)_2$] and Ca-Sr-hydroxyapatite [$\text{Ca}_2\text{Sr}_8(\text{PO}_4)(\text{OH})_2$] (Fig. 1C, upper spectrum: double and single arrow indicates peaks characteristic for whitlockite and $\text{Ca}_2\text{Sr}_8(\text{PO}_4)(\text{OH})_2$ respectively). The occurrence of whitlockite in this precipitate was confirmed by the presence of magnesium in this sample using Electron Probe X-ray Micro Analysis (EPXMA) (Fig. 1E).

A similar observation was made for the XRD analysis of the synthetic hydroxyapatite samples (Fig. 1B and D). Here the mineral doped with 0, 0.6 and 3.2% Sr was

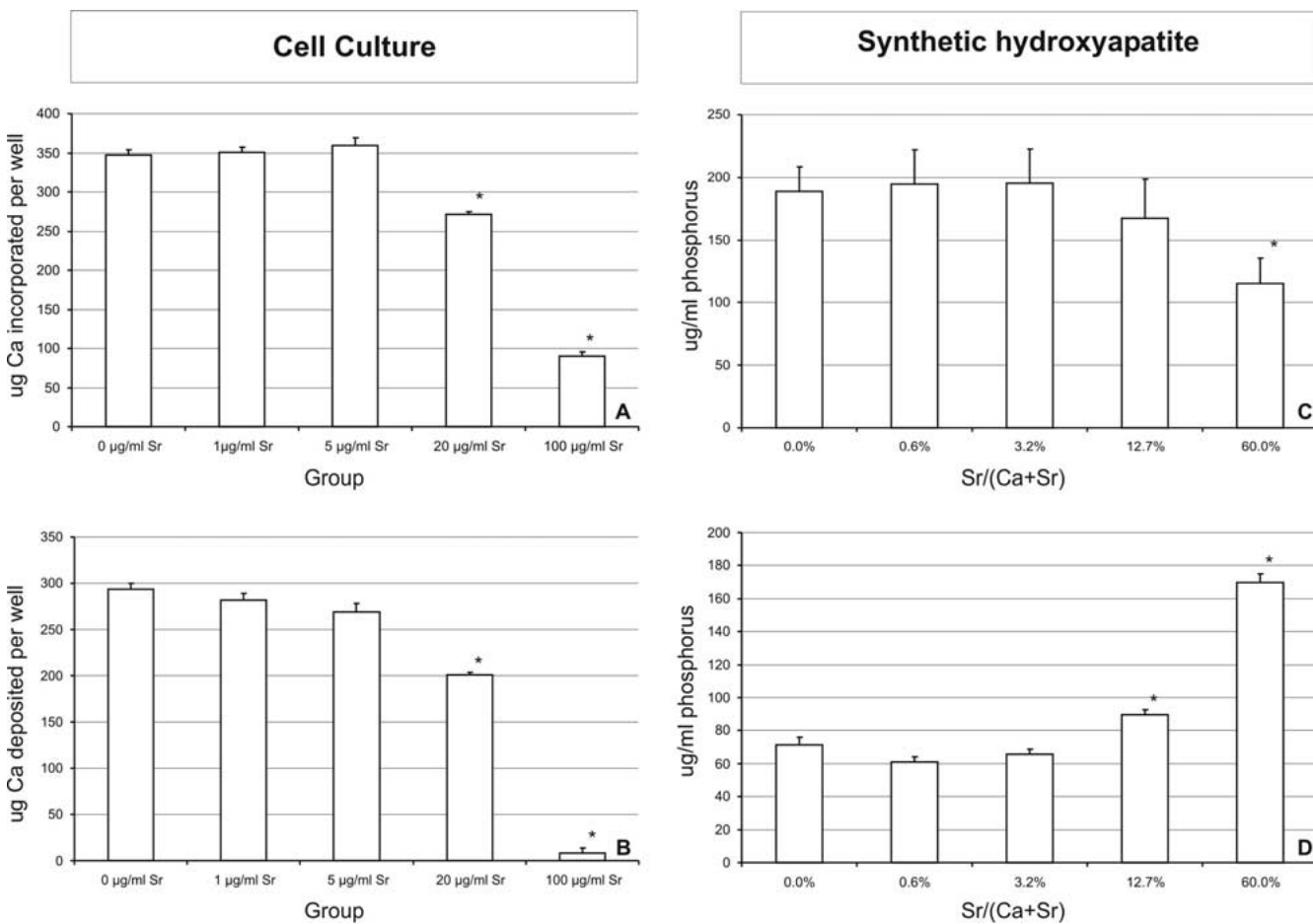


Fig. 4. Ca-incorporation expressed as area under the time-incorporation-curve (A) and Ca-deposition (B), both in the cell culture, show a significantly reduced mineralization for the highest Sr-groups (20 and 100 µg/ml Sr). Phosphorus consumption demonstrates a significantly diminished crystal

identified as Ca-hydroxyapatite using the same powder-diffraction database. The apatite doped with 12.7% Sr was identified as $\text{Ca}_9\text{Sr}(\text{PO}_4)_6(\text{OH})_2$, while the 60% mineral was identified as $\text{Ca}_3\text{Sr}_7(\text{PO}_4)_6(\text{OH})_2$. Comparable to the XRD-pattern of the mineralized cell cultures treated with 100 µg/ml Sr, a diffuse background was observed in the XRD-pattern of the synthetic hydroxyapatite containing 60% Sr, indicating a reduced crystallinity and/or the presence of an amorphous phase. The integrated XRD-spectra of both the mineral deposited in the cell culture exposed to the highest Sr concentration (100 µg/ml) and the synthetic hydroxyapatite with 60% Sr/(Sr + Ca) showed a clear shift of the major diffraction peaks of the apatitic crystal planes 310, 211 and 002 towards larger interplanar distances (d-spacing; Table 1).

FTIR Analysis

FTIR spectra of the ν_3 (950–1150 cm^{-1}) and ν_4 (500–650 cm^{-1}) vibrations from the PO_4 -domain are pre-

growth in hydroxyapatite containing high Sr-concentrations [60 mol% Sr/(Sr + Ca)] (C). Solubility measured as phosphorus release from synthetic apatite (D) indicates an increased solubility for the apatites contaminated with 12.7 and 60 mol% Sr/(Sr + Ca). (* $P < 0.05$ vs. control group).

sented in Figure 2 for both mineralized cell cultures (2A,B) and synthetic apatites (2C,D), all revealing peaks characteristic for hydroxyapatite. Peaks from the spectra from the cell cultures are less sharp than those from the synthetic apatite samples, indicating the presence of smaller or less crystalline mineral in the cell culture samples. At the highest Sr concentrations corresponding with 100 µg/ml Sr and 60% Sr/(Sr + Ca) in cell culture and hydroxyapatite samples, respectively, markedly less sharp peaks in both the ν_3 and ν_4 domain are observed, indicating a reduced crystallinity and hereby confirming our XRD-results. Deconvolution analysis of the recorded FTIR-spectra also showed a peak shift towards smaller wave numbers in the highest Sr-group for both osteoblast cultures and synthetic apatite samples [100 µg/ml Sr and 60% Sr/(Sr + Ca), respectively]. Due to the severe mineralization defect observed in the cell cultures treated with 100 µg/ml Sr, deconvolution data of the ν_3 -domain were not reliable and as such could not be interpreted correctly. No significant differences were

Table 1. Quantification of crystal lattice expansion of Sr-containing hydroxyapatite expressed as interplanar distances (d-spacing, nm)

| Crystal plane | Cell culture | | Synthetic hydroxyapatite | |
|---------------|-----------------------|-------------------------|--------------------------|------------------|
| | 0 $\mu\text{g/ml}$ Sr | 100 $\mu\text{g/ml}$ Sr | 0% Sr/(Sr + Ca) | 60% Sr/(Sr + Ca) |
| 310 | 2.26 nm | ND* | 2.27 nm | 2.32 nm |
| 211 | 2.78 nm | 2.90 nm | 2.81 nm | 2.89 nm |
| 002 | 3.42 nm | 3.46 nm | 3.42 nm | 3.58 nm |

*ND: Not detectable

found in the amide I and II and in the carbonate domain of hydroxyapatite after deconvolution.

Scanning Electron Microscopy

To confirm both XRD and FTIR analysis, a scanning microscopic study was performed on the various synthetic hydroxyapatite samples. Quantitative results show that the mean crystal size is significantly decreased ($P < 0.05$) in the mineral containing 60 and 100% Sr/(Sr + Ca) (Fig. 5). Together with the reduced crystal size there was an increase in the occurrence of amorphous mineral. Ultimately, in the 100% Sr-apatite sample [i.e., $\text{Sr}_{10}(\text{PO}_4)_6(\text{OH})_2$] no individual crystals but only an amorphous precipitate was present (Fig. 5F).

Discussion

In a previous study the effect of a wide range of Sr concentrations on the *in vitro* bone formation/mineralization was investigated in primary osteoblast cell cultures isolated from fetal rat calvaria. Using this set-up, a complex dose-dependent effect of the element on the *in vitro* bone formation was found [19]. Moreover, it was possible to make a distinction between an inhibitory effect of Sr on the *in vitro* nodule formation in the presence of an intact mineralization at low concentrations and a defective mineralization resulting from a physicochemical interference of the element with the hydroxyapatite formation at high Sr concentrations. These *in vitro* observations were in line with previous observations in a chronic renal failure rat model in which at serum Sr concentrations comparable to those in the culture medium a mineralization defect was seen also [12].

To further elucidate the role of Sr in the development of a mineralization defect, a new *in vitro* study using the UMR-106 rat osteosarcoma cell line was designed. The UMR-106 cell culture system is a widely used model to study the *in vitro* mineralization process [29–31]. These cells actively secrete extracellular matrix in which, upon addition of β -glycerolphosphate, an alkaline phosphatase involved mineralization process occurs [30]. This

cell culture model has the advantage that it allows to produce an adequate amount of mineral which permits to perform detailed XRD- and FTIR-analysis, quite impossible with primary nodule-forming osteoblast cell cultures because of the limited amount of mineral formed *in vitro*, especially at high Sr doses. Using these techniques it was possible to identify the *in vitro* deposited mineral as hydroxyapatite, making this model appropriate for studying the properties of this mineral and the possible effects of particular agents, including Sr on its physicochemical characteristics under physiological conditions.

At high Sr concentrations (20 and 100 $\mu\text{g/ml}$ Sr) the clearly reduced mineralization, indicated by both the Ca-incorporation and Ca-deposition, in combination with a normal alkaline phosphatase activity is indicative for a direct interference of the element with hydroxyapatite formation pointing to a behavior similar to that previously observed in primary osteoblast cultures treated with the same Sr concentrations [19]. This suggestion is further supported by the results of the solubility and crystal growth experiments obtained with the Sr-contaminated synthetic hydroxyapatite samples, clearly showing the presence of a physicochemical interference of Sr with the hydroxyapatite formation at concentrations of 12.7 and 60% Sr/(Sr + Ca). Furthermore, the solubility and crystal growth experiments confirm the previous findings reported by Christoffersen et al. [24] demonstrating an increased hydroxyapatite solubility and decreased crystal growth in the presence of Sr [24]. In the latter publication the authors investigated the effects of relatively low Sr concentrations [0–10% Sr/(Sr + Ca)] on the physicochemical properties of synthetically prepared hydroxyapatite. They found a significantly reduced crystal formation and increased solubility at 10% Sr/(Sr + Ca). The authors further suggested that the substitution of Ca by Sr causes a crystal lattice expansion due to the larger atomic radius of Sr which in turn alters the solubility of the mineral. This suggestion is supported by the results of the present study, in which the peak shift in both XRD and FTIR spectra (ν_3 and ν_4 vibrations of the phosphate domain) is indicative of a substantial expansion of the crystal

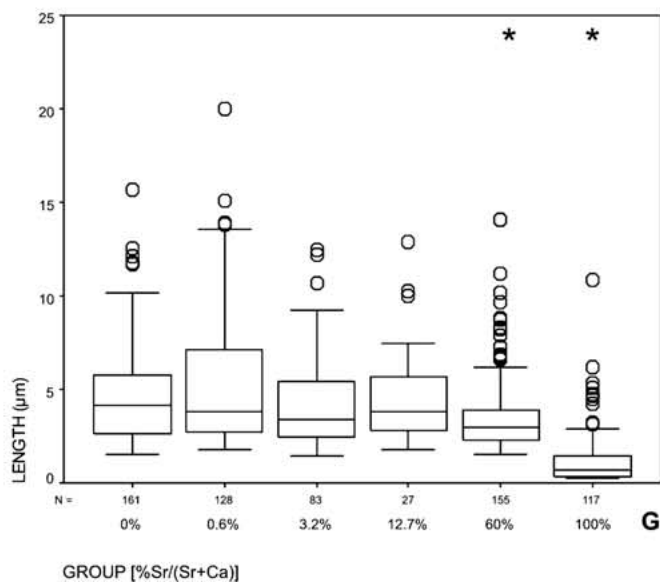
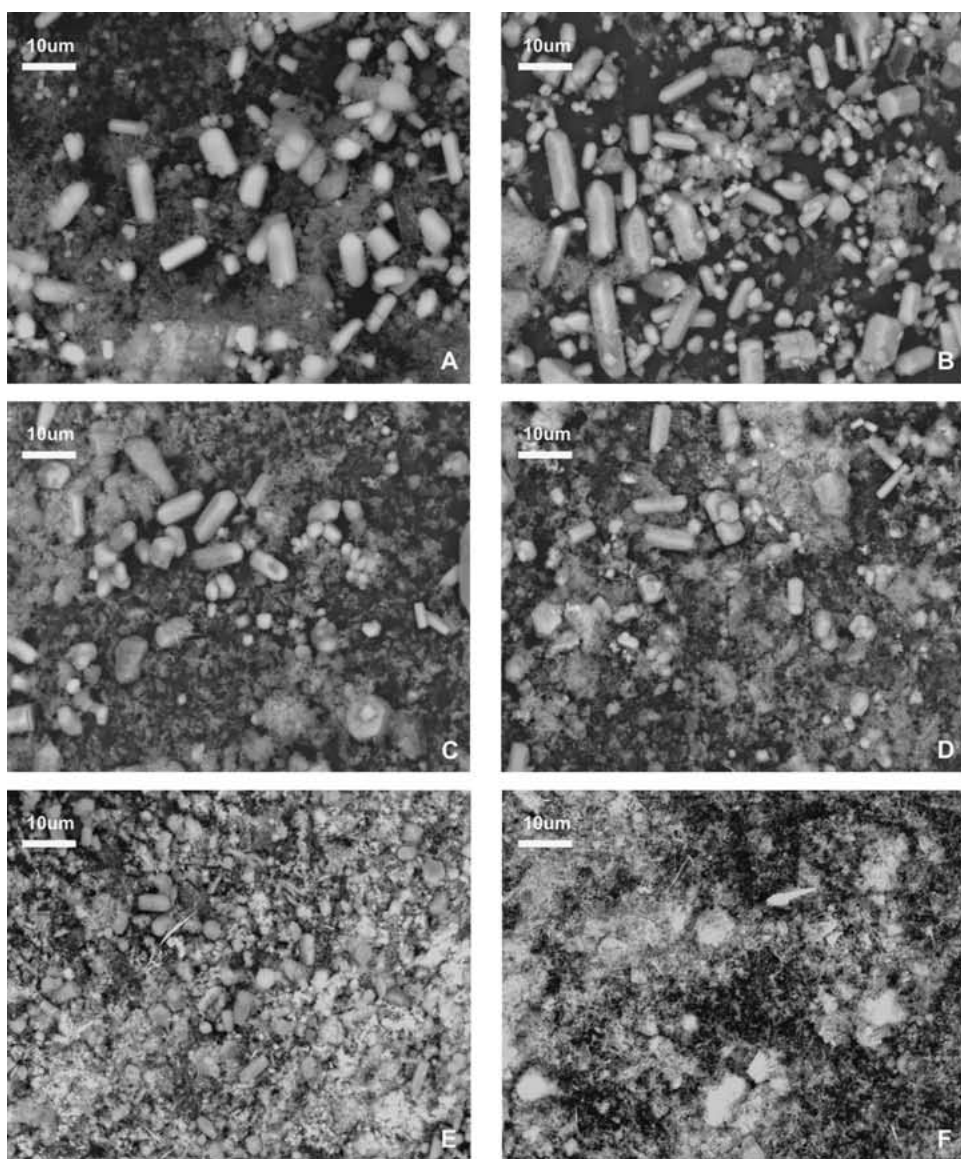


Fig. 5. Scanning electron microscopic image of synthetic hydroxyapatite doped with 0 (A), 0.6 (B), 3.2 (C), 12.7 (D), 60 (E) and 100 mol% Sr/(Sr+Ca) (F) indicating the decreasing mineral size in the presence of high Sr content (bar represents 10 μ m). Quantification of the crystal sizes presented on boxplots revealed a significant reduction in crystal length in the samples containing 60 and 100% Sr/(Sr+Ca) ($*P < 0.05$ vs. the other groups) (G).

lattice dimensions at the highest Sr groups of both cell cultures and synthetic minerals. These effects only occur when Sr is incorporated into the apatite crystal lattice by heteroionic substitution, thereby replacing Ca [32].

Although, by the availability of various techniques, it has become possible to present evidence for the existence of a physicochemical interference of Sr with the hydroxyapatite formation in both synthetic hydroxyapatite and mineralizing cell cultures, still no data are available that show of evidence the role of such a mechanism in the *in vivo* development of a mineralization defect either in the presence of chronic renal failure or normal renal function. In this context, it has to be emphasized that the above-mentioned physicochemical interference of Sr at a concentration of 100 $\mu\text{g}/\text{ml}$ in cell culture and at 60% Sr/(Sr+Ca) in synthetic hydroxyapatite is substantially above the concentration found *in vivo* in animals as well as humans loaded with the element.

Boivin et al. [33] as well as our group [12] previously reported that Sr is heterogeneously incorporated in bone with 2 to 3 times more Sr in new than in old bone. Given the serum Sr concentrations in chronic renal failure rats loaded with 0.15% Sr²⁺ in the drinking water during 12 weeks, varying around 11 $\mu\text{g}/\text{ml}$ and corresponding with bulk bone Sr concentrations of 2.3 mol% Sr/(Sr+Ca) [13], one may reasonably expect local bone Sr concentrations of 5–7% Sr/(Sr+Ca). Even at these local concentrations, it is very unlikely that the observed osteomalacia in these animals is the solely result of a physicochemical interference of Sr with the hydroxyapatite formation. In the presence of chronic renal failure, PTH secretion, vitamin D metabolism and Ca/P homeostasis are seriously disturbed, resulting in a stimulated bone turnover and histological characteristics of hyperparathyroidism. This altered bone metabolism and Ca homeostasis may contribute to the increased susceptibility of bone to the development of Sr-induced osteomalacia in patients with an impaired renal function. In osteoporotic patients treated with 1–2 g Sr-ranelate/day, serum Sr-concentrations may increase to levels in the range of 10–15 $\mu\text{g}/\text{ml}$, corresponding to a bulk bone Sr-content of 1.6–3 mol% Sr/(Sr+Ca) [34]. Taking into account the heterogenic anatomy of bone one may expect that *in situ*, depending on its localization, local Sr-concentrations reaching values up to 3–9 mol% may occur. However, up to now no mineralization defect or signs of osteomalacia in these patients have been reported so far. In the present study a reduction in synthetic hydroxyapatite crystal size could be demonstrated using SEM (Fig. 5A vs. 5D) at comparable Sr-concentrations and was also previously reported by Christoffersen et al. [24]. This latter effect is not necessarily an adverse effect since it is suggested by others that bone strength is inversely related to crystallinity of the bone mineral [35, 36]. The smaller the

crystals the greater the total crystal surface, the better the bone rigidity. Hence, reduction in the bone mineral crystallinity can be one of the explanations of the observed increase of bone strength in Sr-treated osteoporosis patients [32]. In the line of this, FTIR studies by Paschalis et al. revealed that the skeleton of osteoporotic patients contains more mature/crystalline mineral and thus larger hydroxyapatite crystals which contributes to the brittleness of the bone [35, 36]. However, until now no data presenting evidence for such an effect of Sr-treatment on the bone mineral to occur *in vivo* have been provided. This is not surprising in view of the notion that to the best of our knowledge all previous crystallographic measurements (XRD) were performed on pulverized bone samples, hereby averaging out local effects of the element [33, 37]. To further elucidate the effect of Sr on the *in vivo* mineral crystallinity, crystallographic studies on a μm scale such as micro-small-angle-X-ray-scattering (μSAXS) and micro-X-ray-diffraction (μXRD) on bone biopsies of patients loaded with Sr should be performed in the near future.

The discrepancy between the effects of Sr on bone in either the presence or absence of a normal renal function cannot be explained by the physicochemical interference of the element with the hydroxyapatite formation. Most likely, chronic renal failure induces some major metabolic changes in the calcium homeostasis by which the bone metabolism becomes more susceptible to the adverse effects of Sr at the level of bone formation and mineral deposition. However, getting a better insight in the exact mechanisms responsible for this discrepancy is beyond the scope of the current study; however, it will be the subject of future investigations.

The exact sense of the presence of whitlockite in the cell cultures treated with the highest Sr concentration (100 $\mu\text{g}/\text{ml}$ Sr) is not very clear. Because it only represents very low amounts of mineral, indicated by the low intensity of the bands in the XRD pattern and the very low Ca-deposition, it is likely a side effect of the Sr-induced mineralization defect where a nonspecific precipitate under the form of whitlockite is deposited. With regard to the physiological importance of this mineral, only an association with articular cartilage calcifications has been made so far in the literature [38, 39].

In conclusion, in the present paper, evidence for a direct physicochemical interference of Sr with the hydroxyapatite formation is presented in both an *in vitro* osteoblast cell culture system and in synthetic hydroxyapatite. The physicochemical effect of the element on the hydroxyapatite is expressed by a reduction in mineral crystal size (both in cell culture and in synthetic hydroxyapatite) which at high concentrations ultimately results in an impaired mineralization. The biological impact in the *in vivo* situation of such an effect still remains ambiguous and needs further investigations *in vivo* at the μm scale.

Acknowledgments. We acknowledge the European Synchrotron Radiation Facility for provision of synchrotron radiation facilities and we would like to thank Michael Drakopoulos and Andrea Somogyi for assistance in using beamline ID18F. P. Cool acknowledges the FWO-Vlaanderen (Fund for Scientific Research Flanders) for financial support.

References

- Rosenthal HL, Eves MM, Cochran OA (1970) Common strontium concentration of mineralized tissues from marine and sweet water animals. *Comp Biochem Physiol* 32:445–450
- Schroeder HA, Tipton IH, Nason AP (1972) Trace metals in man: strontium and barium. *J Chronic Dis* 25:491–517
- Rosenthal HL, Cochran OA, Eves MM (1972) Strontium content of mammalian bone, diet and excreta. *Environ Res* 5:182–191
- Skoryna SC (1984) Metabolic aspects of the pharmacologic uses of the trace elements in human subjects with specific reference to stable strontium. *Trace Subst Environ Health* 18:3–23
- Grynepas MD, Hamilton E, Cheung R, Tsouderos Y, Deloffre P, Hott M, Marie PJ (1996) Strontium increases vertebral bone volume in rats at a low dose that does not induce detectable mineralization defect. *Bone* 18:253–259
- Marie PJ, Garba MT, Hott M, Miravet L (1985) Effect of low doses of stable strontium on bone metabolism in rats. *Miner Electrolyte Metab* 11:5–13
- Marie PJ, Hott M, Modrowski D, De Pollak C, Guillemain J, Deloffre P, Tsouderos Y (1993) An uncoupling agent containing strontium prevents bone loss by depressing bone resorption and maintaining bone formation in estrogen-deficient rats. *J Bone Miner Res* 8:607–615
- Matsumoto A (1988) Effect of strontium chloride on bone resorption induced by prostaglandin E2 in cultured bone. *Arch Toxicol* 62:240–241
- Omdahl JL, DeLuca HF (1972) Rachitogenic activity of dietary strontium. I. Inhibition of intestinal calcium absorption and 1,25-dihydroxycholecalciferol synthesis. *J Biol Chem* 247:5520–5526
- Omdahl JL, DeLuca HF (1971) Strontium-induced rickets: metabolic basis. *Science* 174:949–951
- Ozgun S, Sumer H, Kocoglu G (1996) Rickets and soil strontium. *Arch Dis Child* 75:524–526
- Schrooten I, Behets GJ, Cabrera W, Vercauteren SR, Lamberts LV, Verberckmoes SC, Bervoets AJ, Dams G, Goodman WG, De Broe ME, D'Haese PC (2003) Dose-dependent effects of strontium on bone of chronic renal failure rats. *Kidney Int* 63:927–935
- Schrooten I, Cabrera W, Goodman WG, Dauwe S, Lamberts LV, Marynissen R, Dorrine W, De Broe ME, D'Haese PC (1998) Strontium causes osteomalacia in chronic renal failure rats. *Kidney Int* 54:448–456
- Grynepas MD, Marie PJ (1990) Effects of low doses of strontium on bone quality and quantity in rats. *Bone* 11:313–319
- Meunier PJ, Reginster JY (2003) Design and methodology of the phase 3 trials for the clinical development of strontium ranelate in the treatment of women with postmenopausal osteoporosis. *Osteoporos Int* 14(suppl)3:66–76
- Meunier PJ, Slosman DO, Delmas PD, Sebert JL, Brandi ML, Albanese C, Lorenc R, Pors-Nielsen S, De Vernejoul MC, Roces A, Reginster JY (2002) Strontium ranelate: dose-dependent effects in established postmenopausal vertebral osteoporosis—a 2-year randomized placebo-controlled trial. *J Clin Endocrinol Metab* 87:2060–2066
- Reginster JY, Meunier PJ (2003) Strontium ranelate phase 2 dose-ranging studies: PREVOS and STRATOS studies. *Osteoporos Int* 14(suppl)3:56–65
- Reginster JY (2002) Strontium ranelate in osteoporosis. *Curr Pharm Des* 8:1907–1916
- Verberckmoes SC, De Broe ME, D'Haese PC (2003) Dose-dependent effects of strontium on osteoblast function and mineralization. *Kidney Int* 64:534–543
- Tietz NW, Rinker AD, Shaw LM (1983) IFCC methods for the measurement of catalytic concentration of enzymes Part 5. IFCC method for alkaline phosphatase (orthophosphoric-monoester phosphohydrolase, alkaline optimum, EC 3.1.3.1). *J Clin Chem Clin Biochem* 21:731–748
- Hansen AC (1973) Atomic absorption spectrophotometry for calcium and magnesium in serum and urine. *Absorption Newslett* 12:125–128
- D'Haese PC, van Landeghem GF, Lamberts LV, Bekaert VA, Schrooten I, De Broe ME (1997) Measurement of strontium in serum, urine, bone, and soft tissues by Zeeman atomic absorption spectrometry. *Clin Chem* 43:121–128
- Sun J, Xue M, Kikuchi M, Akao M, Aoki H (1994) Effects of Sr-hydroxyapatite microcrystal on cultured cell. *Bio-med Mater Eng* 4:503–512
- Christoffersen J, Christoffersen MR, Kolthoff N, Barenholdt O (1997) Effects of strontium ions on growth and dissolution of hydroxyapatite and on bone mineral detection. *Bone* 20:47–54
- Fiske CH, Subbarow Y (1925) The colorimetric determination of phosphorus. *J Biol Chem* 66:375
- Wess T, Alberts I, Hiller J, Drakopoulos M, Chamberlain AT, Collins M (2002) Microfocus small angle X-ray scattering reveals structural features in archaeological bone samples: detection of changes in bone mineral habit and size. *Calcif Tissue Int* 70:103–110
- Somogyi A, Drakopoulos M, Vincze L, Vekemans B, Camerani C, Janssens K, Snigirev A, Adams F (2001) ID18F: a new micro-X-ray fluorescence end-station at the European Synchrotron Radiation Facility (ESRF) preliminary results. *X-ray Spectrometry* 30:242–252
- Hammersley AP, Svensson SO, Hanfland M, Fitch AN, Hausermann D (1996) Two-dimensional detector software: from real detector to idealised image or two-theta scan high pressure. *Research* 14:235–248
- Schneider GB, Zaharias R, Stanford C (2001) Osteoblast integrin adhesion and signaling regulate mineralization. *J Dent Res* 80:1540–1544
- Stanford CM, Jacobson PA, Eanes ED, Lembke LA, Midura RJ (1995) Rapidly forming apatitic mineral in an osteoblastic cell line (UMR 106-01 BSP). *J Biol Chem* 270:9420–9428
- Chak CW, Lee KM, Leung KS, Fung KP (1995) A change in bone-specific alkaline phosphatase activities in cultured rat osteoblastic cells under L-ascorbate and beta-glycerophosphate-induced mineralization. *Cell Biol Int* 19:979–985
- Marie PJ, Ammann P, Boivin G, Rey C (2001) Mechanisms of action and therapeutic potential of strontium in bone. *Calcif Tissue Int* 69:121–129
- Boivin G, Deloffre P, Ferrat B, Panczer G, Boudeulle M, Mauras Y, Allain P, Tsouderos Y, Meunier PJ (1996) Strontium distribution and interactions with bone mineral in monkey iliac bone after strontium salt (S 12911) administration. *J Bone Miner Res* 11:1302–1311
- Dahl SG, Allain P, Marie PJ, Mauras Y, Boivin G, Ammann P, Tsouderos Y, Delmas PD, Christiansen C (2001) Incorporation and distribution of strontium in bone. *Bone* 28:446–453
- Paschalis EP, Betts F, DiCarlo E, Mendelsohn R, Boskey AL (1997) FTIR microspectroscopic analysis of human iliac crest biopsies from untreated osteoporotic bone. *Calcif Tissue Int* 61:487–492
- Paschalis EP, Betts F, DiCarlo E, Mendelsohn R, Boskey AL (1997) FTIR microspectroscopic analysis of normal

- human cortical and trabecular bone. *Calcif Tissue Int* 61:480–486
37. Boivin G, Meunier PJ (2003) The mineralization of bone tissue: a forgotten dimension in osteoporosis research. *Osteoporos Int* 14(suppl)3:19–24
 38. Ryan LM, Cheung HS, LeGeros RZ, Kurup IV, Toth J, Westfall PR, McCarthy GM (1999) Cellular responses to whitlockite. *Calcif Tissue Int* 65:374–377
 39. Scotchford CA, Ali SY (1997) Association of magnesium whitlockite crystals with lipid components of the extracellular matrix in human articular cartilage. *Osteoarthritis Cartilage* 5:107–119
 40. Aronow MA, Gerstenfeld LC, Owen TA, Tassinari MS, Stein GS, Lian JB (1990) Factors that promote progressive development of the osteoblast phenotype in cultured fetal rat calvaria cells. *J Cell Physiol* 143:213–221
 41. Bhargava U, Bar-Lev M, Bellows CG, Aubin JE (1988) Ultrastructural analysis of bone nodules formed *in vitro* by isolated fetal rat calvaria cells. *Bone* 9:155–163
 42. Nefussi JR, Brami G, Modrowski D, Oboeuf M, Forest N (1997) Sequential expression of bone matrix proteins during rat calvaria osteoblast differentiation and bone nodule formation *in vitro*. *J Histochem Cytochem* 45:493–503